Detection and Mapping of Cover Crops Using Sentinel-1 SAR Remote Sensing Data

Sami Najem, Nicolas Baghdadi, Hassan Bazzi, Nathalie Lalande, and Laurent Bouchet

***Abstract*—Cover crops are intermediary crops planted in between two main cash crops. They play a role in limiting nitrate leaching into groundwater. Currently, there is no database pertaining to cover crops despite their importance. The development period of cover crops is characterized by a dense cloud cover in Europe, which obstructs land surface monitoring using optical remote sensing. This study proposes a cover crops mapping method based on synthetic aperture radar remote sensing data from the Sentinel-1 (S1) constellation, which is unaffected by weather conditions. Our method is based on the dynamics of the S1 backscattering coefficient at the plot level. Using a decision tree, we mapped cover crops. In the decision tree algorithm, filters were added to eliminate other crops that temporally intersect with the cover crop, namely wheat and rapeseed. The proposed decision tree proved effective in detecting existing cover crop plots, as shown by the classification Recall values ranging between 83.5% and 95.0% and the high precision values ranging between 81.5% and 89.2%. Comparison with the Random Forest classifier showed that our proposed method yielded better and more consistent results. The main limitations in the classification approach were weak cover crops and residual vegetation. The results show that the developed approach, based on the S1 time series, is capable of remotely monitoring cover crops, giving managers and decision makers the ability to follow farmers' work and ascertain if they are applying the recommended agricultural practices that promote sustainable land use and limit the contamination of groundwater.**

***Index Terms*—Cover crops, groundwater, synthetic aperture radar (SAR) remote sensing, Sentinel-1 (S1), sustainable land use.**

I. Introduction

THE world's population is increasing rapidly, leading to higher demand for food resources. This growing demand begets a need to improve agricultural productivity, resulting in more intense exploitation of agricultural land [1], [2] and in an increased use of chemical fertilizers. Unfortunately, when not managed correctly, excess fertilizers move through the soil profile and reach the groundwater table causing the contamination of the groundwater table with nitrates [3], [4]. This happens through a process called nitrate leaching, leading to negative health impacts on communities, caused by the contamination of drinking water sources [5], and to environmental harm to aquatic ecosystems, caused by the high concentration of nitrates [6], [7]. Leaching is influenced by many factors such as leaching potential, soil characteristics, irrigation practices [8], [9], and agricultural practices (fertilizer inputs, tillage). One of the practices commonly used to reduce nitrate infiltration into the groundwater is cover cropping [10], [11], [12].

Cover cropping can be a powerful tool for promoting healthy soil and sustainable agriculture practices [13], [14]; it is a part of the conservation agriculture practices (along with zero tilling and mulching) that are applied by farmers around the world [15]. The primary functions of cover crops include limiting nutrient leaching, mitigating soil erosion, and enhancing long-term soil fertility [16], [17], [18], [19]. The influence of cover crops arises from their ability to minimize the loss of nitrates, nutrients, and sediment from agricultural fields [20], [21] because they act as a barrier, hindering the movement and transfer of materials [22]. Hence, they can capture nutrients during the winter months that will later be released at the start of the growing season of the subsequent main crop [23]. In fact, cover crops are proven to be effective in reducing nitrate leaching [24]. Other than reducing nitrate leaching, cover crops also limit soil erosion and weed growth through competition. Wood and Bowman [25] found that cover crops have impacts on four soil health indicators (active carbon, aggregate stability, respiration, and total organic matter). On a larger scale, cover crops play an important role in water conservation at the basin level by protecting groundwater from pollution [26]. Conversely, the absence of cover cropping leads to nutrient leaching since soils are exposed following the harvest of main crops. Cover crops are sown subsequent to the harvest of a field, serving the purpose of providing soil coverage to enhance the agroecosystem. They are fast-growing crops, grown between successive plantings of a main crop. In our study areas (located in the west of France), cover crops are planted from mid-August to mid-October, after summer crops (maize, sunflower, etc.) or after winter crops (wheat, rapeseed, etc.), and then harvested (plowed) before planting the next crop from mid-November to end-March, depending on planting time if the following crop. Effective cover crop management involves careful planning, proper timing, and attention to detail.

Manuscript received 1 August 2023; revised 7 November 2023; accepted 23 November 2023. Date of publication 30 November 2023; date of current version 14 December 2023. This work was supported in part by the French Space Study Center (CNES, TOSCA 2023), in part by the National Research Institute for Agriculture, Food and the Environment, and in part by Envilys. *(Corresponding author: Sami Najem.)*

Sami Najem is with the TETIS, CIRAD/CNRS/INRAE, INRAE, Université de Montpellier, 34000 Montpellier, France (e-mail: sami.najem@inrae.fr).

Nicolas Baghdadi is with the UMR-TETIS, INRAE, 34093 Montpellier, France (e-mail: nicolas.baghdadi@inrae.fr).

Hassan Bazzi is with the Atos France, Technical Services, 95870 Bezons, Paris, France (e-mail: hassan.bazzi@atos.net).

Nathalie Lalande and Laurent Bouchet are with the R&D, Envilys, 34750 Villeneuve les Magulonne, France (e-mail: nathalie.lalande@envilys.com; laurent.bouchet@envilys.com).

Digital Object Identifier 10.1109/JSTARS.2023.3337989

The Nitrates Directive (91/676/EEC) was adopted in 1991 by the United Nations. It has two objectives: the first is to reduce water pollution caused by nitrates and eutrophication from agricultural activities and the second is to prevent the spread of such pollution. From 2012 on, winter soil cover became mandatory for all farms in vulnerable zones (a vulnerable zone, is a part of the territory, defined by the Nitrates Directive as water pollution by the direct or indirect discharge of nitrates of agricultural origin threatens in the short term the quality of aquatic environments and more particularly drinking water supply). Furthermore, over the last two decades, the EU Water Framework Directive (Directive 2000/60/EC) has been advocating the use of cover cropping as a measure to safeguard water bodies against excessive fertilization. The European legislative guidelines on the Common Agricultural Policy (EU Regulation No 1307/2013) have provided the primary legal framework for on-site monitoring and the requirement for comprehensive information on cover cropping areas. These EU-level legislations along with numerous other national and local level legislations ("Nitrates directive") adopted in 1991 aim to reduce water pollution caused by nitrates from agricultural sources. In 2011, these measures were expanded in France through the sixth "nitrates" action program consisting of a national action program, containing mandatory measures for all French vulnerable zones. Moreover, there are regional (department level or drinking water catchment supply area) action programs that are adapted to each territory that reinforce certain measures taken on the national level with additional actions in order to achieve the water quality objectives. These legislations elevated the importance of the monitoring and detection of cover cropping throughout the European region, leading to the increased interest in modern, technologically advanced tools that allow for the monitoring of large areas quickly and affordably, most notably remote sensing data.

Remote sensing data has been widely employed for the monitoring of vegetation covers [27], [28]; it offers advantages such as the relatively few resources needed when compared to traditional field visits, and the ability to have large-scale applications when needed. Optical remote sensing is a very important tool for quantitatively assessing vegetation abundance [29]. Through the analysis of reflected light across various spectral bands, optical remote sensing enables the extraction of essential information pertaining to vegetation characteristics and dynamics. Indices, such as the normalized difference vegetation index (NDVI) [30], facilitate the precise quantification of vegetation density and health [31], [32]. Optical multispectral remote sensing has been used for estimating crop areas by generating crop type maps and conducting crop classification [33], [34], [35]. Furthermore, it has proven valuable for assessing various plant-biophysical characteristics, such as the green leaf area index and canopy-level chlorophyll content among others [36], [37]. Prabhakara et al. [38] studied the relationship between ten different visible range and near-infrared indices and the percent ground cover and biomass of winter cover crops were compared, showing that the NDVI was strongly correlated with the percent groundcover ($r2 = 0.93$) and that the triangular vegetation index was best and used high ranges of biomass ($r2 = 0.86$). The European Sentinel-2 (S2) constellation, in particular, produces free and open access data with a high spatial resolution ranging from 10 m to 60 m (10 m $\times$ 10 m for the bands used for NDVI) as well a high temporal resolution (five days revisit time). These characteristics allow for its use in crop detection as well as the mapping of changes in land use throughout the growing season with a high overall accuracy higher than 90% [39], [40]. S2 data were also utilized for mapping of cover crops with an overall accuracy of over 84% [41].

A significant challenge for optical remote sensing data in monitoring the seasonal dynamics of crops during winter arises from the limited availability of cloud-free optical images in the northern hemisphere. To overcome this limitation, synthetic aperture radar (SAR) data offer a reliable alternative. SAR is a remote sensing technology that uses microwave radiation to take scans of Earth's surface. During cloudy months, SAR images enable the study of intra-annual vegetation changes because they are unaffected by atmospheric conditions [42].

Since vegetation affects the SAR backscattered signal according to its density and the geometric structure of its components (leaves, stems, and fruit), there is a direct link between the SAR backscattering mechanisms and characteristics of the vegetation cover [43], [44], [45]. The European Sentinel-1 (S1) SAR data have a high spatial resolution (pixel spacing of 10 m $\times$ 10 m) and a high temporal resolution (six days revisit time). For crop monitoring, SAR data could be used in a complementary fashion with optical images [46], [47], except in regions with persistent cloud cover (tropical and equatorial zones) where radar data are exclusively used. In a study proposed by Minh et al. [48], deep learning techniques were applied for winter crop detection using the S1 time-series, achieving an overall accuracy higher than 90%. In their study, they used vertical–horizontal (VH) and vertical–vertical (VV) polarizations in order to identify the density of the vegetation cover, without discriminating winter crops from cover crops. The vegetation was split into five classes from bare soil to high-density vegetation. They obtain the best performances in the high-density class and the lowest performances in the low-density class.

Seeing the potential of SAR in vegetation monitoring and since optical remote sensing data is not reliably available in the winter months, the aim of this study is to map cover crop fields using S1 SAR data. S1 time series were used in order to extract the radar signal from each agricultural field in the VV and VH polarizations. In addition to these raw channels, additional channels based on the mean S1 signal at the grid scale (5 km $\times$ 5 km) were used in order to reduce the soil contribution from the total S1 signals. The classification method we developed at the plot scale is a multilevel decision tree that classifies the fields based on criteria from multiple S1 channels. The classification method eliminates fields that have other types of vegetation during the same period as the cover crops (wheat and rapeseed). The final classification indicates whether the field had a cover crop or not. Finally, the result of our decision tree will be compared to the results of the Random Forest (RF) classifier, which is a commonly used machine learning classifier.

II. Materials and Methods

A. Study Sites

We conducted this study in the Charente-Maritime Department in the west of France. The arable surface makes up 64% of the total area in this department. Fig. 1 shows the location of the two examined sites, the first had an area of around 500 km^2

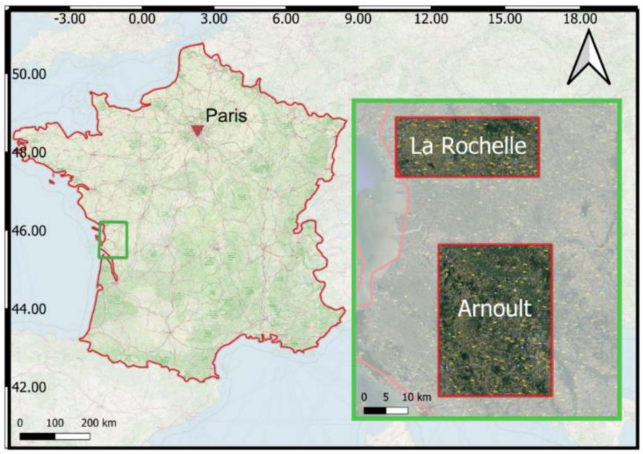

Fig. 1. Location of our two study sites.

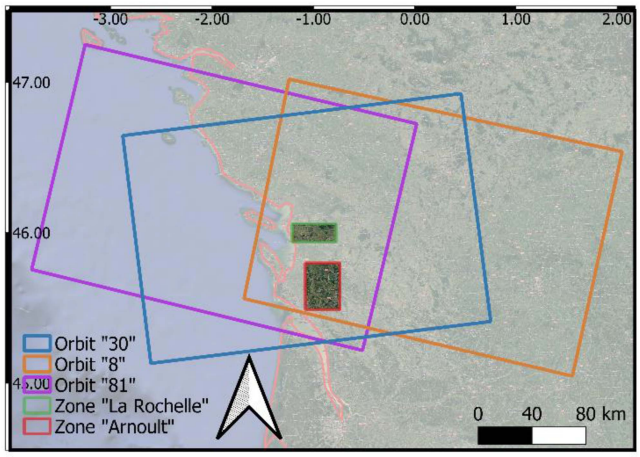

Fig. 2. S1 orbits used in this study.

near the city of La Rochelle and the second had an area of around 900 km^2 and is located near the city (commune) of Saintes in the watershed of Arnoult River, referred to hereafter as "Arnoult." The climate in this region is oceanic with around 1000 mm of rainfall and 2000 h of sun annually. The principal crop types in the area are wheat, maize, sunflower, and rapeseed. For example, according to the farmer's declarations of the year 2018 (https://geoservices.ign.fr/rpg), 26.8% of the agricultural field in the study sites had wheat, 22.1% had maize, 8.9% had sunflower, and 2.3% had rapeseed. In the two study sites, cover crops are cultivated either between one summer crop (usually maize or sunflower) and one winter crop (cereal, usually wheat) or between two summer crops (maize or sunflower). Generally, in this region, cover crops are planted by mid-October at the latest and harvested by mid-November at the earliest. The harvesting date of cover crops depends on the following crop. If the next crop is a winter crop, then the cover crops will be harvested early [from mid-November of the first year (Y1) to end-December of the next year (Y2)]. However, if the next crop is a summer crop, then the cover crop will be harvested from the beginning of February to end-March of the second year (Y2).

B. Sentinel-1 Remote Sensing Data

For this study, we used a time-series of Sentinel 1A and Sentinel 1B satellite-captured C-band SAR images (5.405 GHz). All the available acquisitions were utilized consisting of the "ascending" (evening at 18:00 UT) and "descending" (morning at 06:00 UT) acquisitions. Fig. 2 shows the extent of the orbits used in this study.

We used both the VV and VH polarizations from every acquisition. S1 images have a spatial resolution of 10 m $\times$ 10 m. The data are available freely on the European Space Agency's (ESA) website (https://scihub.copernicus.eu/dhus/#/home). We downloaded and processed S1 data from 2017 to 2021. The number of orbits used, as well as the number of S1 images, is detailed in Table I. The data were calibrated using the ESA S1 toolbox. The radiometric calibration is the first step in the calibration process; it is the processing of transforming the data from a digital number into a backscattering coefficient σ in linear units. The second type of correction is orthorectification; it is the geometric correcting of the SAR images using a digital elevation model at 30 m from the shuttle radar topography mission as a topographical reference.

TABLE I
NUMBER OF ORBITS IN EACH YEAR AND THE TOTAL NUMBER OF CORRESPONDING S1 IMAGES PER YEAR

Year	Total number of orbits	Total number of S1 images	Average number of images per month
2017	3	178	15
2018	3	181	15
2019	3	163	14
2020	3	179	15
2021	3	178	15

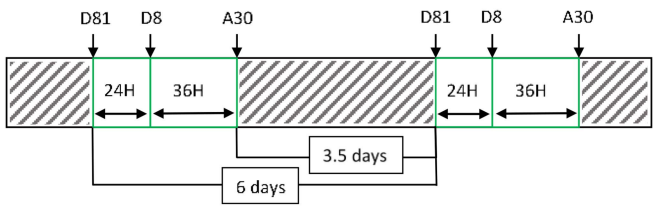

Fig. 3. Frequency of S1 images in "ascending" (A) and "descending" (D) for all orbits covering our study sites. The hatched area represents the period with no S1 acquisitions.

All the acquired images were stacked regardless of the acquisition orbit. For each reference field, an S1 acquisition dataset was built consisting of three orbits. Fig. 3 shows the temporal distribution of the S1 orbits over our study site. The first acquisition is a "descending" image belonging to the orbit 81 (D81). The following image comes 24 h later and is a descending acquisition as well, this time, from orbit 8 (D8). Then, the third acquisition comes 36 h later as an ascending acquisition from orbit 30 (A30).

Six days after the first image, the cycle repeats in the same way with a new D81 image. The hatched area in Fig. 3 represents the 3.5-day period that separates every bunch of three images (D81, D8, and A30) from the next. The incidence angles for our study sites were between 23° and 38° for orbit 81 and between 32° and 48° for both orbits 8 and 30.

After calibration, every S1 image offers two outputs, an image of the backscattering coefficient in the VV polarization and an image of the backscattering coefficient in the VH polarization. Thus, our times-series of S1 images results in two basic resulting time-series: the VV time-series and the VH time-series. In addition, we created a new time-series that is the difference between the VH and the VV values at every date, called the VH–VV times-series.

In order to work on the field scale, we averaged the pixels in each reference field, obtaining a single representative value for each field. The end results of this process were three time-series at the field level (marked with a "p") VVp, VHp, (VHp−VVp).

In addition to S1 images, all cloud-free S2 optical images over each study site/year were downloaded from the Theia website (https://www.theia-land.fr/). The S2 images provided by Theia are corrected for atmospheric interference and so are called Level-2A products. S2 images were mainly used to calculate the NDVI time series. Our approach developed in this study does not use optical data. However, NDVI data calculated from S2 images were used to better understand the phenological cycle of the different reference fields visited during the field surveys.

C. In Situ Data

The in situ database consists of field observations on the type of crop on numerous reference fields. The field surveys were performed in the years 2017, 2018, 2019, and 2020 between October and December of each year. Field observations were mainly provided from the ReadyNov PollDiff Captages collaborative project led by Envilys Dev and financed by European EAFRD funds and the Occitanie Region (2018–2021). For the La Rochelle site, 1066 observations were available (one observation = one field) compared to 919 observations for the Arnoult site. Around 40% of the dataset is marked as having a cover crop between two main crops.

The French registry for agricultural fields [Registre Parcellaire Graphique (RPG)] was used to correctly delineate the boundary of all agricultural plots in our study area. It is produced on a yearly basis. The RPG is available for download on the French state's GeoServices website (https://geoservices.ign.fr/rpg). For each year in the study period, the corresponding RPG was used.

D. Classification Method

In addition to the S1 time series at the plot scale, VVp, VHp, and VHp−VVp additional layers calculated from S1 images were produced. Given that the S1 signal can show strong fluctuations with changes in soil moisture mainly due to rainfall [49], reducing these fluctuations caused by soil moisture in the S1 signal would be useful in order to better monitor the phenological cycle of cover crop and extract only the vegetation contribution in the S1 backscattered signal. In a study by Bazzi et al. [50], they showed that radar signal averaged at the grid scale (5–10 km^2) is strongly correlated with rainfall events. They demonstrated that between two consecutive S1 images, the main increase/decrease in the S1 signal at the grid scale is mainly due to the presence/absence of rainfall events between these two S1 dates. In their study, they used the differences between the S1 SAR signal calculated at grid scale (representing only rainfall effects) and that calculated at plot scale to remove the rainfall–irrigation ambiguity and detect irrigation events at plot scale [50], [51], [52]. Following the same logic, and in order to remove the effect of rainfall contribution in the S1 backscattered signal at plot sale, we proposed subtracting the plot scale from the grid scale S1 signal. Thus, the following additional channels were produced VVp−VVg, VHp−VHg, and (VHp−VVp)–(VHg−VVg) (the latter channel is called (VH−VV)p−g). The S1 signal at grid scale was calculated by averaging the backscattering coefficient of all agricultural pixels with an NDVI value below 0.4 in each grid cell of 5 km × 5 km. Using agricultural pixels with NDVI less than 0.4 ensures that the calculated backscattered signal at 5 km × 5 km is only affected by the soil moisture variation (mainly rainfall) and has no high vegetation contribution. Thus, for each polarization and grid cell, the average backscatter coefficient was obtained (marked with a "g"). The average signal over each grid cell reflects the soil moisture conditions of the cell; therefore, any rainfall events at the grid level will be detectable. Finally, four new channels were calculated VVp−VVg, VHp−VHg, and (VHp−VVp)–(VHg−VVg). This latter channel is called (VH−VV)p−g.

Furthermore, using the difference between channels (e.g., VHp−VVp, VHp−VHg, and VVp−VVg) reduces the effect of incidence angle. In fact, the radar signal depends on the incidence angle, it decreases when the incidence angle decreases. For example, the radar signal for a given target can be up to 2 dB weaker with an incidence angle of 48° (the lowest incidence on our site) than with an incidence angle of 23° (the highest incidence on our site) [53]. The difference between channels also highlights the contribution of vegetation and amplifies the difference between vegetation covers and bare soil by subtracting the effect of the bare soil (represented by the grid-level data).

Smoothing was then applied to every channel using the Gaussian smoothing method, allowing us to detect the maximums (peaks) and minimums in our time series. The dates of the peaks were located by following the dynamic of the time series and retrieving the dates at which the amplitude of the time series at the date t is bigger than the amplitude at the date $t-1$ and also bigger than that at $t+1$. The dates of the minimums are located by following the opposite strategy, with the amplitude at time t being smaller than the amplitude that precedes at $t-1$ and also smaller than the one that follows at $t+1$.

In order to distinguish rapeseed fields using our classification approach, we used the main peak that characterizes the rapeseed between 1 April and mid-June in the S1 time series VHp−VHg [54], [55]. In fact, during the rapid spring growth of rapeseed between April and June, a strong increase in VHp−VHg is observed corresponding to stem elongation, inflorescence

emergence, and fruit development [56]. Thus, normalization and Gaussian fitting were applied to the VHp−VHg channel in order to detect the characteristic peak of the rapeseed. First, a normalization was performed using the min–max normalization method

$$N\_(\mathrm{VHp}-\mathrm{VHg})\ (i) = \frac{(\mathrm{VHp}-\mathrm{VHg})\ (i)-\min(\mathrm{VHp}-\mathrm{VHg})}{\max(\mathrm{VHp}-\mathrm{VHg})\ -\min(\mathrm{VHp}-\mathrm{VHg})}$$

where $N\_(\mathrm{VHp}-\mathrm{VHg})\ (i)$ is the *i*th normalized data. After normalization, a Gaussian curve fitting was performed on the *N*_(VHp−VHg) channel in order to find and register the peaks (position of Gaussians) as well as the minimums.

Finally, we created a database for all the S1 channels processed containing the position and the amplitude of each maximum and minimum.

Each crop type has an S1 time series with a specific behavior, depending on its phenological cycle and on vegetation characteristics (e.g., vegetation water content, biomass, structure). This temporal variability in backscattering coefficients between crops opens a perspective to identify and classify the crops, based on their temporal S1 footprint. Thus, the dynamic signature of the backscattering coefficients of different crops constitutes the basis of our classification approach, which will use the decision tree technique. It is a decision tree consisting of simple "yes" or "no" decisions at every decision node. Each decision node relies on one of the backscattering characteristics of the crops. Attributes such as the approximate sowing and harvesting dates and the date of maximum growth (high biomass), among others, were used at every node in the decision tree in order to progressively eliminate crops other than cover crops and reach a final classification of cover crop and not a cover crop. Each step in the decision tree leads bifurcated branch; in most cases, one of these two branches is a limiting pathway, ending the process and deciding that the plot is not a cover crop.

Fig. 4 is an example of all the S1 time series (6 channels) used in this study in order to build our classification approach. Fig. 4(a) shows the dynamic of VHp−VVp over a cover crop plot through time. Within the red frame, we find one peak of VHp−VVp and two surrounding minimums, showing the full development and then the recession of the cover crop, with the beginning (minimum before the peak), the maximum growth (peak), and the end (minimum that follows the peak) of the cover crop life cycle. In our study sites, planting of cover crops usually begins in mid-August to mid-October of the first year (Y1) and the harvesting occurs from 1 November of the first year (Y1) to end-March of the second year (Y2). In order to correctly classify cover crops, our detection method uses S1 time series between 1 May Y1 and end-June Y2 in order to follow the development of all crops in the study region not only the cover crops because we also need to distinguish temporally overlapping and adjacent crops, such as wheat and rapeseed, from the cover crop.

For the detection of cover crops, we will use S1 time series between 1 May Y1 and end-June Y2. This range of S1 dates is necessary in order to detect the fields with cover crops while eliminating other overlapping crops that are shown in Fig. 4 since the VHp–VVp is the channel that follows most clearly the development of cover crops (the (VV−VH)p−g channel also well represents the vegetation development but we chose the VHp-VVp channel because it requires fewer layers). The first step in our decision tree is to check if we have a peak in VHp−VVp (a maximum resulting from the smoothing of the VHp–VVp channel) in our period of interest from 15 September Y1 to 31 March Y2 (the period within which we have the peak of the cover crops growth, starting approximately one month after sowing) in blue in Fig. 4.

If we do have at least one peak, we continue to the next step in our decision tree. The rest of the decision tree will be applied to every peak found within this period. Next, our decision tree is split into two main branches: one for detecting "early" cover crops with a cultivation period in our study sites between 15 September Y1 and 31 January Y2 and one for detecting "tardy" cover crops with a cultivation period between 1 February and 31 March Y2. For the early cover crops branch, we will then look if the peak detected is in January of Y1 and if the difference in amplitudes between this peak and the minimum before it is less than 0.5 dB (these two conditions are strongly linked to cereal crops).

If both of these conditions are met, the field is classified as not a cover crop [indicating probably wheat, Fig. 5(a)]; if one or both of these conditions are not met, we proceed to the next level in the decision tree. For the tardy cover branch, we check if we have a minimum in the VHp−VHg channel between 1 April and end-June; this condition was used because cereal crops show a distinctive dip in the VHp−VHg channel during this period caused by the emergence of heads in these crops. If this condition is met, the plot is characterized as not cover crops [indicating probably wheat, Fig. 5(b)]; if this condition is not met, we proceed to the next level in the decision tree (possible cover crop). The two branches reunite at the next level in the decision tree. In the next step in our decision tree, we check the presence of two minimums in VHp–VVp (the channels that best follow cover crop development), one minimum before the peak (from the 1 May to the day of the peak) and also one minimum after the peak (from the day of the peak to end-June). In fact, the minimum that is before the peak indicates the end of the preceding crop (allowing for the planting of the cover crop), while the minimum that is after the peak signifies the end of the cover crop cycle. If both of these minimums are present, we can continue to the next step in our decision tree (possible cover crop).

For the next and final step in our decision tree, in order to eliminate any ambiguity with rapeseed, we look for multiple conditions. First, we look if we have a peak in the normalized and Gaussian fitted VHp−VHg from 1 April to 15 June Y2 since that is when the strongest signal from rapeseed in the VHp−VHg channel is observed (this channel best shows fruit development, right after the flowering stage). Second, we examine to see if this peak has the highest amplitude in the time series with a normalized amplitude that is superior to 0.6 (this condition is necessary to have for a rapeseed crop). Third, we look for a lack of a minimum in (VH−VV)p−g between 1 Feb to end-March Y2 (if present, this minimum would indicate that this is not, in fact,

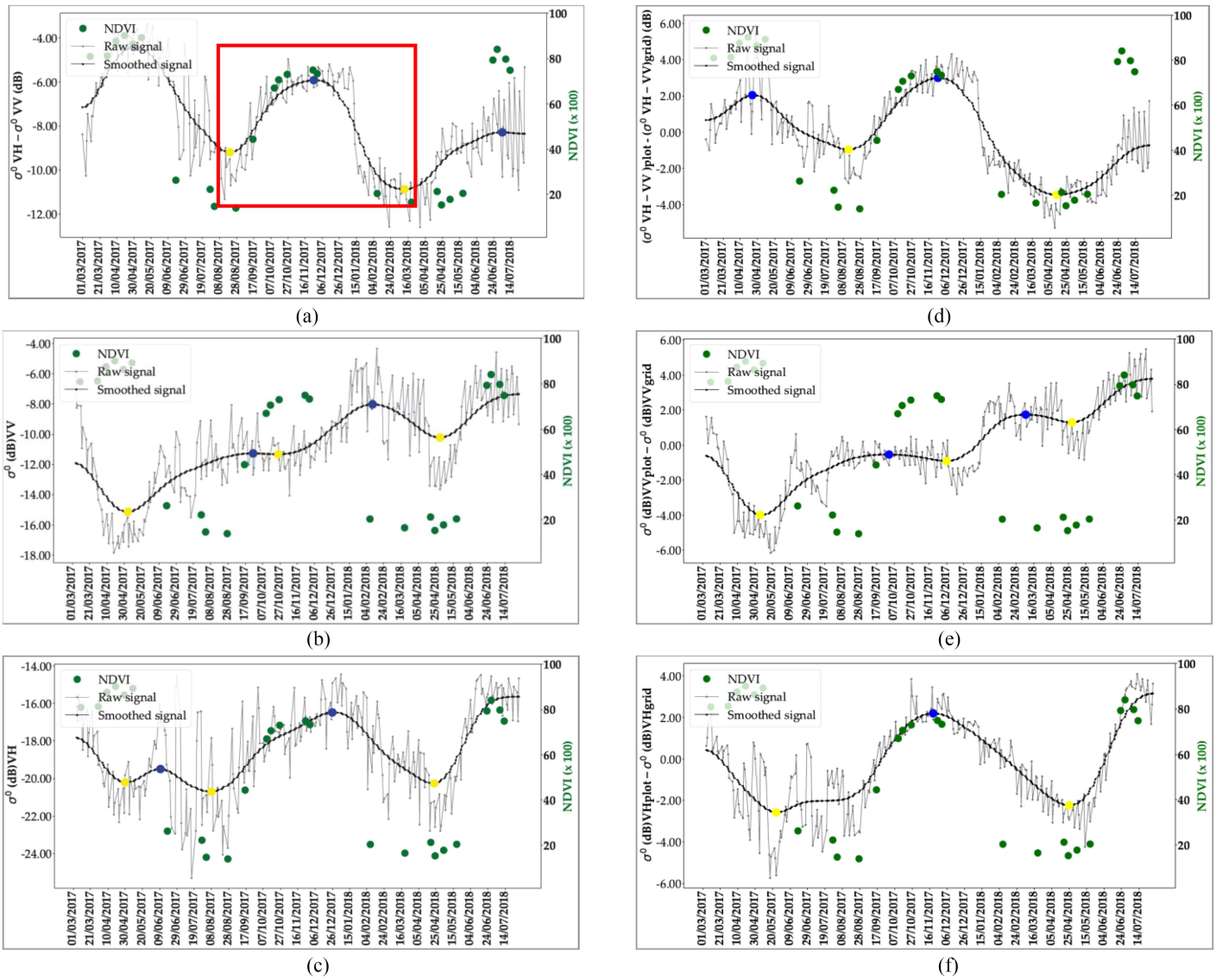

Fig. 4. S1 time series examples for a cover crop plot showing the raw signal and the smoothed signal. The blue and yellow points are respectively the maximum "peaks" and the minimum in our S1 time series for (a) VHp−VVp, (b) VVp, (c) VHp, (d) (VV−VH)p−g, (e) VVp−VVg, and (f) VHp−VHg. In addition, NDVI values calculated from S2 images are plotted.

rapeseed crop) or the presence of a minimum with an amplitude lower than 0 dB (in this case, the minimum is not considered as a true minimum and is insignificant). If these conditions were met, that signals the possible presence of a rapeseed culture [see Fig. 5(c)]. If one or all of these conditions were not met, then we classify the field as having a cover crop. Fig. 6 shows the decision tree, detailing every step.

In addition, we will also use the RF classifier in order to compare the results of our proposed classifier with this commonly used classifier

E. Accuracy Metrics

In order to measure the reliability of our method, we used common classification metrics that measure the skill of our decision tree at detecting the presence of cover crops on one hand, and our ability to distinguish between cover crops and temporally intersecting or adjacent crops. For this purpose, we used the recall, precision, and Kappa metrics, comparing the results of our classification method to the collected ground truth data. Table II lists the description and equation of these accuracy metrics.

III. Results

A. Classification Accuracy

The results of the classification are presented by sites "La Rochelle" and "Arnoult" and by growing season. For example, for a given site, during the 2017–2018 growing season, cover crops can be planted from mid-August to mid-October 2017 and harvested from mid-November to end-March 2018, so we are classifying cover crops using data from both years (we look

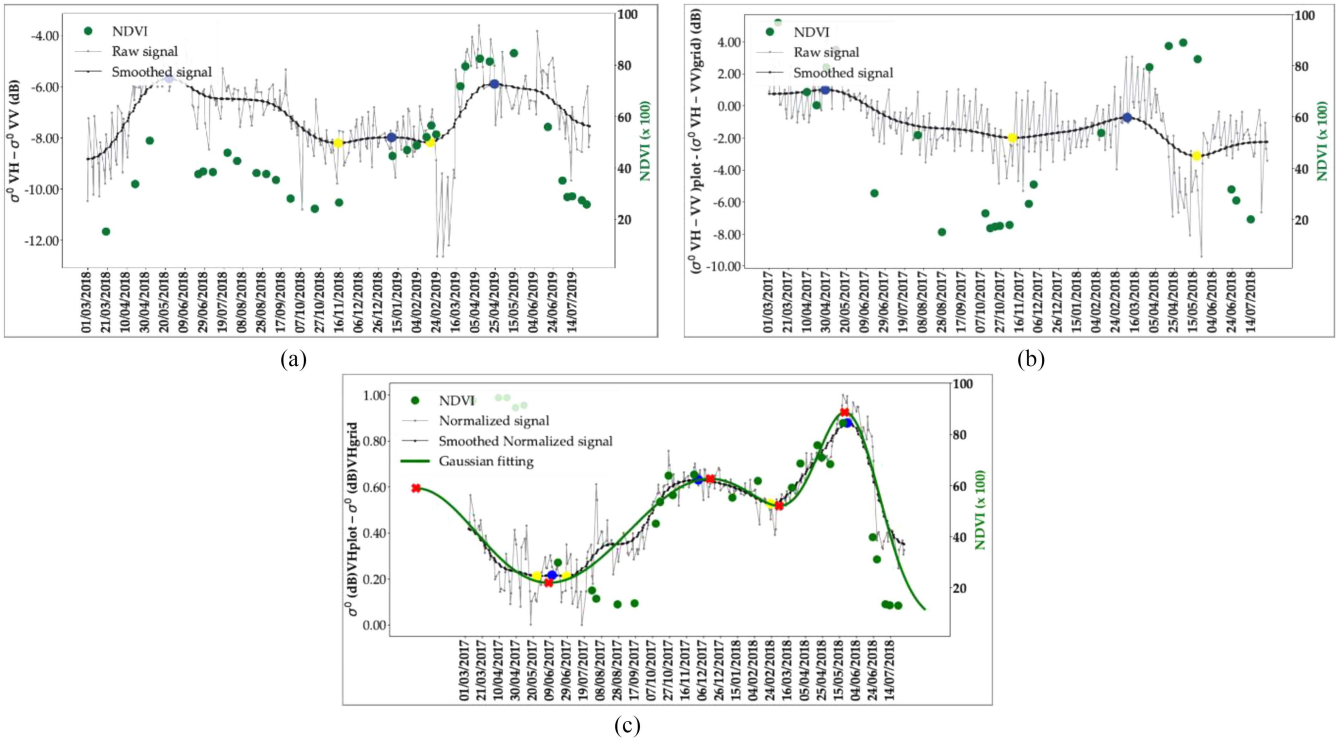

Fig. 5. S1 time series examples for (a) wheat plot in the VHp−VVp channel showing Delta peak − min < 0.5 dB; (b) wheat plot in the (VH−VV)p−g showing a minimum between 1 April and end-June, (c) rapeseed plot showing a peak in Normalized and Gaussian fitted VHp−VHg (seen in green) from 1 April to 15 June Y2.

TABLE II
DESCRIPTION OF THE ACCURACY METRICS USED IN THIS STUDY

Metric	Description	Equation	Reference
Recall	Recall shows the proportion of the positive classes in the ground samples that are detected in the results. Meaning that it shows the algorithm's ability to detect all positive (cover crop) cases.	$\frac{TP}{TP+FN}$	[57]
Precision	Precision shows the proportion of the detected positive classes in the results that are actually correct. Meaning it examines if all the fields classified as cover crops are in fact cover crops.	$\frac{TP}{TP+FP}$	[57]
Kappa	Kappa compares the likelihood of agreement to what would be expected if the ratings were independent. The values range from -1 to 1, with 1 representing perfect agreement and 0 representing no agreement or independence.	$\frac{2*((TP*TN)-(FN*FP))}{(TP+FP)*(FP+TN)+(TP+FN)*(FN+TN)}$	[55]

for a peak of VHp−VVp from 15 September 2017 to end-March 2018). Table III illustrates the accuracy of our results compared to ground truth. It shows the Recall, Precision, Kappa, User's accuracy, and Producer's accuracy values of our method for every growing season from 2017–2018 to 2020–2021 and for each of our study sites.

For the «La Rochelle» site, the Recall value ranges from 83.5% for the 2017–2018 season to 95.0% for the 2020–2021

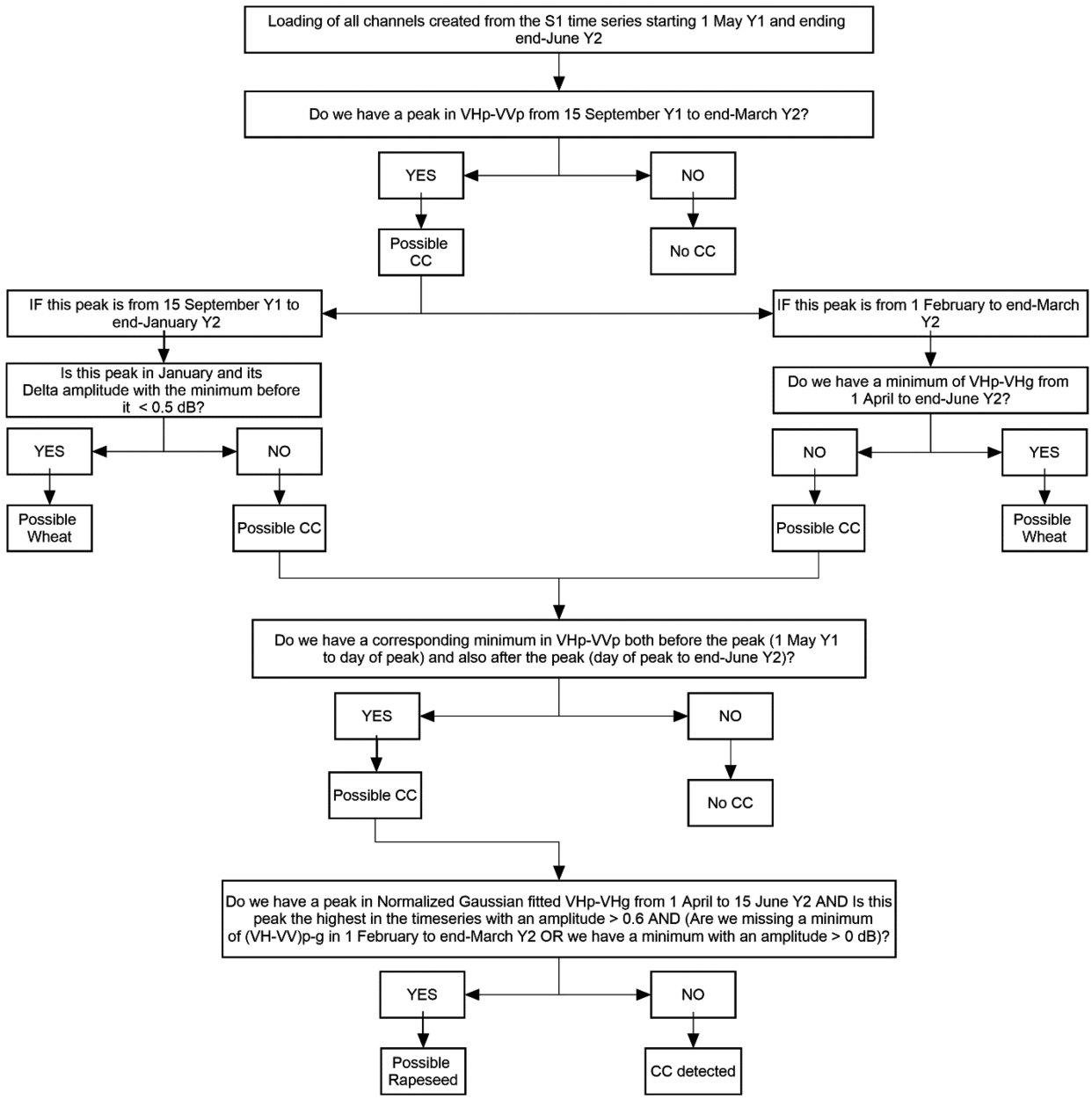

Fig. 6. Diagram of our proposed cover crop mapping approach based on the decision tree. This decision tree is applied to every peak located within the 15 September Y1 to 31 March Y2 time period (cover crop presence period). "peaks" and "minimums" refer respectively to the maximums and the minimums that are detected in the S1 time series after Gaussian smoothing. Delta amplitude = amplitude of peak − amplitude of minimum. CC: Cover crops.

season, while the Precision ranged from 89.1% for the 2018–2019 season to 88.3% in the 2020–2021 season and Kappa ranges from 0.76 in the 2019–2020 to 0.89 in the 2020–2021 seasons.

In the «Arnoult» site, Recall ranges from 84.6% in the 2019–2020 season to 91.4% in 2018–2019, Precision ranges from 81.5% for the 2018–2019 season to 87.9% in the 2017–2018 season, and Kappa ranged from 0.72 in 2019–2020 to 0.83 in the 2017–2018 seasons.

The average recall values for all four growing seasons were around 90.6% for the «La Rochelle» site with an average precision of around 87.8% and an average Kappa of around 0.83. While in the «Arnoult» site, the average recall is around 86.9% with an average precision of 84.8% and an average Kappa of around 0.78. Overall, for both study sites and all growing seasons, the average recall value was around 88.9%, the average precision value was around 86.4%, and the average Kappa value was around 0.80.

B. Mapping of Cover Crops

In order to monitor and better understand cover cropping in our study sites, we applied our classification method to all agricultural fields (except vineyards, orchards, and grasslands)

TABLE III
RECALL, PRECISION, AND KAPPA VALUES OF OUR METHOD FOR EACH YEAR OF THE STUDY FOR EACH SITE

Site	Year	2017-2018	2018-2019	2019-2020	2020-2021
La Rochelle	Recall	83.5%	90.2%	91.5%	95.0%
	Precision	89.2%	89.1%	85.3%	88.3%
	Kappa	0.81	0.85	0.76	0.89
	Number of fields	243	305	360	359
Arnoult	Recall	89.5%	91.4%	84.6%	84.9%
	Precision	87.9%	81.5%	85.2%	84.6%
	Kappa	0.83	0.81	0.72	0.78
	Number of fields	192	211	352	307

TABLE IV
PERCENTAGE OF FIELDS WITH COVER CROPS PER YEAR FOR BOTH STUDY SITES

Year	Percentage of classified fields with cover crops
2017-2018	38.1%
2018-2019	33.3%
2019-2020	54.9%
2020-2021	34.1%

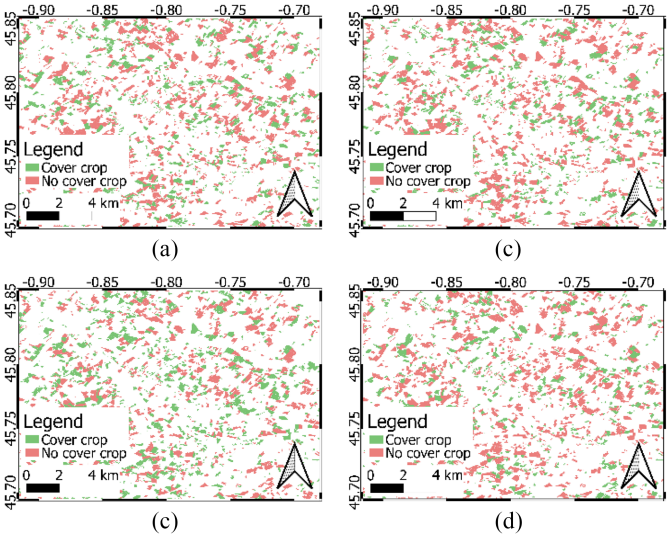

Fig. 7. Subset of cover crop maps from the Arnoult site. (a) 2017–2018 season. (b) 2018–2019 season. (c) 2019–2020 season. (d) 2020–2021 season.

based on the RPG. A subset of cover crop maps from the Arnoult site is shown as an example of the generated cover crop maps in Fig. 7 for the four growing seasons.

TABLE V
PROPORTION OF FIELDS WITH COVER CROPS CONTINUITY OF 0, 1, 2, 3, AND 4 TIMES DURING THE FOUR-YEAR PERIOD

General continuity (out of 4 total years)	Proportion of fields
0 times	13.6%
1 time	37.8%
2 times	32.2%
3 times	13.4%
4 times	3.0%

TABLE VI
PROPORTION OF FIELDS AS A FUNCTION OF COVER CROP PLANTING PATTERN

Planting pattern	Proportion of fields
Two consecutive years	29.3%
Three consecutive years	9.3%
year-on year-off	22.2%

Table IV lists the percentage of fields with cover crops in each growing season for both of our study sites. It varies from 33.3% in the 2018–2019 season to 54.9% in the 2019–2020 season.

C. Temporal Continuity Analysis of Cover Crops

Following the classification of agricultural fields, we performed an analysis of the temporal continuity of cover crops within our study period in order to obtain insight into the planting habits of the farmers. For every classified field, we followed the temporal distribution and the pattern of cover crops within our growing seasons. First, we analyzed the recurrence of cover cropping within our four-year period. Table V lists how many years of cover cropping we have for each field in our four-year time span. Most fields had cover crops in one out of the four years, with 37.8%, whereas only 3.0% of fields had cover crops in four years in a row.

Second, we studied the temporal patterns of cover cropping in our sites. That was accomplished by examining three planting scenarios. The first scenario corresponds to fields having two consecutive years of cover cropping, the second scenario is fields with three consecutive years of cover crops, and the last scenario is year-on year-off cover cropping. As given in Table VI, 29.3% of fields had two consecutive years of cover cropping, while 9.3% of fields had year years of consecutive cover cropping. On the other hand, 22.2% of fields in our study sites show an alternating pattern of cover cropping (one year on, one year off).

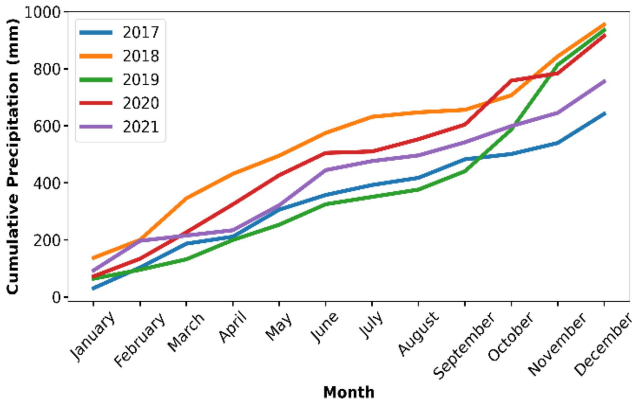

Fig. 8. Cumulative monthly precipitation from 2017 to 2021 (same cumulative precipitation for the two study sites).

IV. Discussion

A. Climatic Zone

Our classification method was applied to all suitable agricultural plots (all agricultural fields except vineyards, orchards, and grasslands) in our study sites (obtained from RPG data). Using the SAR backscatter time series, we aimed to detect the presence of a cover crop at the plot scale. The results show that the classification was successful with an average Recall value of 90.6% on the La Rochelle site and 86.9% on the Arnoult site. The average precision values were 87.8% in the La Rochelle site and 84.8% in the Arnoult site. Finally, the average Kappa scores were 0.83 and 0.78 for La Rochelle and Arnoult, respectively. This shows that there is great potential for cover crop detection using S1 remote sensing data.

Nevertheless, there are some limitations that we will discuss in this section. This cover crop detection method can be used in an agricultural context that is similar to that of our two study sites. In fact, although we do not assume that our approach could be directly applied in all climatic conditions or in sites that are much different from ours, the date intervals selected for each branch of the decision tree are large enough to allow for any shifts that may occur due to local climatic factors. Fig. 8 shows the monthly cumulative precipitation over our study sites for each year from 2017 to 2021. We can see that there is a high interyear variability in precipitation; however, the results of our decision trees remained consistently high throughout the different growing seasons in our study.

However, region-specific adaptation of the thresholds and the intervals of dates used in the decision tree might be required when applied to other regions with different climates, different crop types than those of our study sites, different crop calendars, and different cover cropping practices. For example, dissimilar planting and removal dates of the cover crop in other regions might obligate a shift in the searching window of the minimums and peaks used in the decision tree. However, the signature shape of the S1 signal for the cover crop is expected to remain the same. In addition, in other zones where certain crops (other than wheat and rapeseed) could intersect heavily with the growing season of cover crops, the decision tree should account for those new crops and further levels should be added to filter out those crops.

TABLE VII
Main Reasons False Positives With Their Corresponding Percentage Out of All the False Positives

Reason for the false positives	Percentage
Vegetation residues	80.2%
Soil roughness	15.1%
Weak rapeseed	4.7%

B. Comparison Between Our Proposed Method and the Random Forest Classifier

Compared to other classification methods, such as RF or other machine learning classifiers, our approach based on a decision tree requires no training data before application over a given study site. That being said, comparing our method to RF is important in order to assess the performance of our decision tree.

First, we trained our RF classifier using data from a given study site and growth season and then tested the classifier using another growth season from the same or from another study site. Next, we trained our classifier using all the data from one site (multiyears) and tested it for each growth season in the second study site (see Table VII).

When we use the same study site but at different growing seasons for training and testing (e.g., training La Rochelle 2017–2018 and testing La Rochelle 2018–2019), Recall values ranged between 52.6% and 88.7% for the La Rochelle study site (see Table VI). For the Arnoult site, the Recall values were between 25.3% and 83.8% (see Table VI). As given in Table VI, the best results for the RF classifier arose from using the same site in the test and in the training datasets. In these cases, Recall remained generally high (although in one case it dipped strongly to 25.3% for Arnoult and 43.3% for La Rochelle). When we used different study sites for training and testing (e.g., training La Rochelle 2017–2018 and testing Arnoult 2018–2019), Recall values were between 5.4% and 76.6%. In fact, for these combinations of datasets used in the training and testing, the Recall scores were generally low, with a high variability in the Recall scores between the different combinations. These results indicate an inconsistency in the classification using the RF classifier. In addition to the recall values, Tables VIII and IX list the precision and Kappa values for the RF classifier. Both the precision and Kappa follow the same trend as that of the recall regarding the inconsistency of the RF classifier as well as the high variability of the scores among the different growing seasons and sites.

Second, Table VII also lists the RF classification result when using all the data (multiyears) from each of our two sites as training, then applying it for each growing season of the other study site. The results show recall scores between 44.7% and 73.1%. These scores indicate an improvement in recall score stability over using only one growing season as training.

Comparing the RF classifier's results with the results of our decision tree shows that more often than not, our proposed method yielded better results compared to the results of the RF classifier. In fact, other than in a few results of RF, where we used the same site as train and test, our decision tree-based

TABLE VIII
PRECISION RESULTS FOR RF CLASSIFIER USING DIFFERENT COMBINATIONS AS TRAIN-TEST

			Train: La Rochelle					Train: Arnoult				
			2017-18	2018-19	2019-20	2020-21	Multi years	2017-18	2018-19	2019-20	2020-21	Multi years
Test	La Rochelle	2017-18		74.2%	57.8%	69.1%		38.1%	83.3%	67.1%	21.2%	53.9%
		2018-19	67.7%		68.6%	49.76		34.5%	93.2%	69.7%	16.6%	59.2%
		2019-20	88.2%	81.4%		82.3%		52.8%	92.2%	76.5%	33.3%	74.2%
		2020-21	83.1%	68.3%	86.6%			27.2%	85.6%	34.8%	22.7%	47.5%
	Arnoult	2017-18	69.6%	56.0%	49.3%	44.8%	46.4%		79.1%	69.8%	39.5%	
		2018-19	89.5%	85.6%	46.7%	46.5%	55.7%	44.3%		60.0%	58.1%	
		2019-20	82.2%	73.3%	70.1%	62.5%	72.1%	58.6%	87.8%		65.4%	
		2020-21	94.5%	30%	44.3%	36.5%	42.8%	47.6%	65.6%	65.4%		

TABLE IX
KAPPA RESULTS FOR RF CLASSIFIER USING DIFFERENT COMBINATIONS AS TRAIN-TEST

			Train: La Rochelle					Train: Arnoult				
			2017-18	2018-19	2019-20	2020-21	Multi years	2017-18	2018-19	2019-20	2020-21	Multi years
Test	La Rochelle	2017-18		0.74	0.45	0.57		0.04	0.41	0.42	0.05	0.36
		2018-19	0.58		0.68	0.50		0.18	0.30	0.27	-0.01	0.41
		2019-20	0.72	0.66		0.83		0.14	0.21	0.43	-0.05	0.53
		2020-21	0.56	0.55	0.66			0.04	0.24	0.15	0.01	0.36
	Arnoult	2017-18	0.22	0.15	0.25	0.19	0.21		0.30	0.46	0.47	
		2018-19	0.05	0.25	0.27	0.37	0.40	0.28		0.55	0.34	
		2019-20	0.18	0.41	0.35	0.23	0.43	0.21	0.51		0.33	
		2020-21	0.08	0.02	0.21	0.11	0.15	0.24	0.42	0.43		

classification consistently outperforms RF by a wide margin and does so without the need for a priori information, lending it even greater importance.

C. False Negative Detections of Cover Crops

Although we did not have a large proportion of false negatives (11.1% with a recall of 88.9%), it is still important to understand the limitations of our proposed method. By analyzing the S1 time series of false negatives as well as their corresponding NDVI time series, the main reason for not detecting a field with a cover crop was found to be the weak vegetation density of the cover crop (based on ground truth and shown by NDVI data). Weak vegetation density means that the vegetation development was not important enough to have a sufficient contribution to the total SAR backscattered signal. The first example [see Fig. 9(a)] shows that the peak was not important enough to be considered a true peak as the deltas were too small (<0.5 dB). The second example [see Fig. 9(b)] shows that the S1 signal was not responsive to the presence of the vegetation cover (the vegetation exists but it is not detectable in the SAR signal). Thus, no peak was detected, and it was not possible for the decision tree to successfully detect the cover crop relying solely on the S1 time series' dynamics. By analyzing the NDVI values of the false negative crops during the peak growing season, Fig. 10 shows that around 85% of the undetected cover crop fields attained a maximum NDVI value that is smaller than 0.42 in the mid-September to end-March period. In contrast, fields that were successfully detected as having cover crops showed an average NDVI value of around 0.8 for the same period with more than 90% of these fields having a maximum NDVI higher than 0.52. Furthermore, around 85% of fields that had a false detection were marked during the field visit as having a weak vegetation cover, and 15% were marked as having medium vegetation by the ground survey team.

D. False Positive Detections of Cover Crops

Three main reasons for false positives (13.6% of the cases with a precision of 86.4%) were observed (a false positive occurs when we classify a field as having cover crops when it does not actually have a cover crop). Table X lists the causes of the false positives, where the main reason is vegetation residues (mulching) accounting for 80.2% of false positive cases. Mulching is a land preservation technique where farmers cover the ground with vegetation in order to prevent excessive water evaporation and to increase soil fertility and ecosystem services. Farmers use it as a type of locally sourced mulch and fertilizer. The presence of vegetation residues postharvesting, mainly from maize and sunflower was the reason behind most false positives. In fact, when there is mulch on the field, it could strongly reflect the SAR signal because of its geometric characteristics, leading

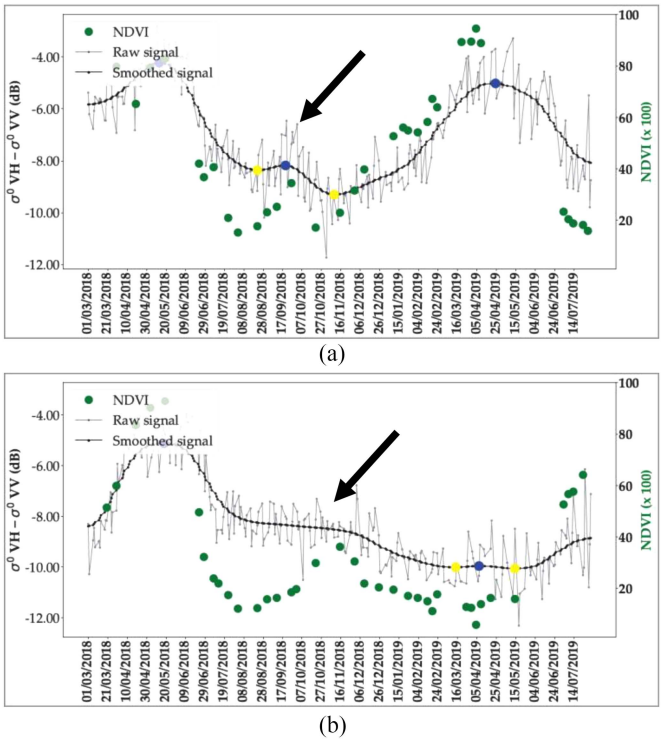

Fig. 9. Examples of S1 time series of false negative fields with their corresponding NDVI showing, (a) weak cover crop with little effect on the S1 time series, (b) weak cover crop with no effect on the S1 time series.

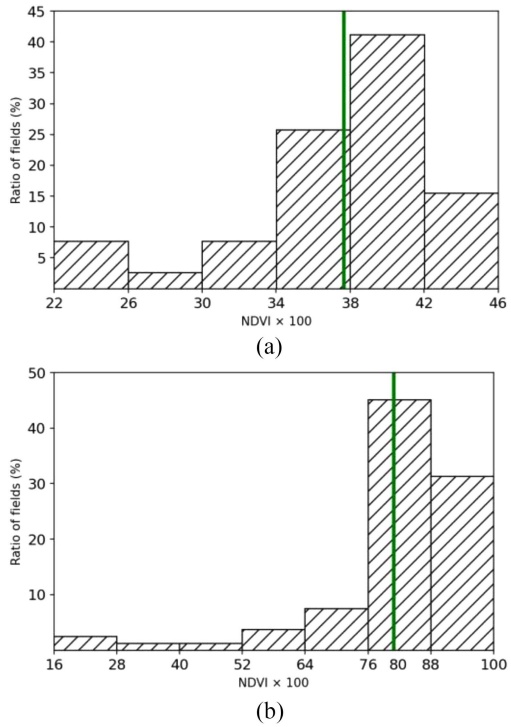

Fig. 10. Histogram showing the percentage of fields as a function of NDVI classes for (a) plots with cover crops that were not successfully classified as such and (b) for successfully detected cover crop fields. The green vertical line shows the mean NDVI value of the distribution.

TABLE X
TOP FIVE MOST COMMONLY CULTIVATED CROPS BEFORE AND AFTER COVER CROPS USING DATA FROM ALL THE YEARS IN OUR STUDY

Preceding crop	Proportion (%)	Following crop	Proportion (%)
wheat	40.5	maize	34.1
maize	21.3	sunflower	18.3
barley	14.0	wheat	13.4
sunflower	7.4	barley	9.7
alfalfa	3.9	peas	8.4

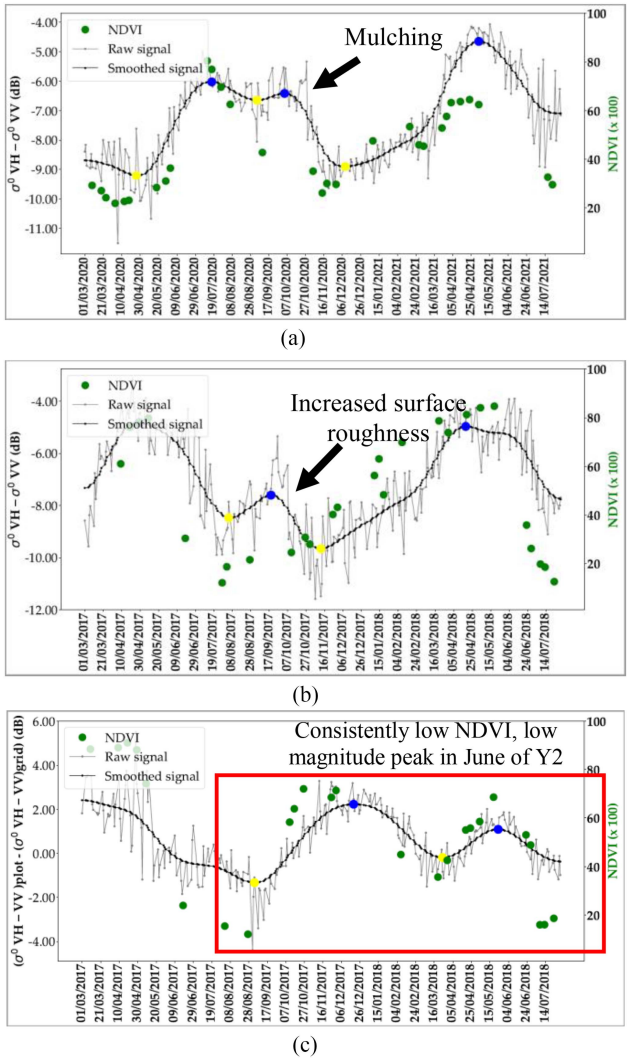

Fig. 11. Examples of S1 time series for false positive detected fields due to (a) residual vegetation, (b) deep plowing, and (c) abnormal rapeseed crop.

to a time series that resembles that of a cover crop field and hence a possible false positive. As shown in Fig. 11(a), after the sunflower harvest in July, the S1 signal stayed at a high magnitude, even when there was no cover crop being grown in the month of October (as shown by the NDVI time series and in situ data).

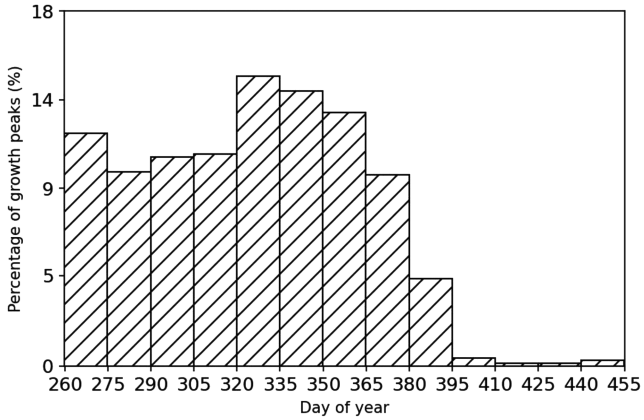

Fig. 12. Distribution of the date of the maximum development of cover crops. DoY = 1 refers to January 1st of year 1, since our study stretches over two calendar years, values above 365 belong to Y2 of every growing season.

The second reason is the increase in soil roughness post plowing. Since the SAR signal is also correlated with soil roughness as shown by Baghdadi et al. [58], deep plowing before sowing also entrains an increase in the reflectance of the SAR signal, which in turn could also lead to a false positive. As shown in Fig. 11(b), an increase in the S1 time series is observed in September caused by an increase in soil roughness following a possible deep plowing. Another 4.7% of false positives were caused by an abnormally weak rapeseed. In these cases, the rapeseed crop was weak enough to be confused with a cover crop (we see the weakness demonstrated in the drop in NDVI in the month of March where it decreased to below 0.4). In that case, the rapeseed filter would not be capable of filtering the rapeseed field, thus resulting in a false positive [see Fig. 11(c)].

E. Maximum Development Date of Cover Crops

With the aim of better understanding the distribution of the date of maximum development of cover crops, Fig. 12 shows this distribution of the day of year (DOY) of the date of maximum growth of every detected cover crop. To detect the maximum growth DOY, we used the peak (maximum growth, detected in the VHp−VVp channel) as a marker. The histogram of Fig. 12 shows that 94.6% of maximum development peaks are between mid-September Y1 (DoY = 260) and mid-January Y2 (DoY = 380). In addition, the distribution of the dates of maximum development shows that about 32.4% of peaks are between mid-September and mid-November (DoY = 320), 62.2% of peaks are between mid-November and mid-January, and less than 10% of peaks are after mid-January Y2.

F. Preceding and Following Crops

In this section, we investigated what crops (top 5) are most likely to precede cover crops and which crops are most likely to follow cover crops using the crop cover classification performed data for all the studied years. Table VIII lists the crops that usually precede (preceding crop) and that usually follow (following crop) a cover crop. It shows that wheat is the most recurrent crop

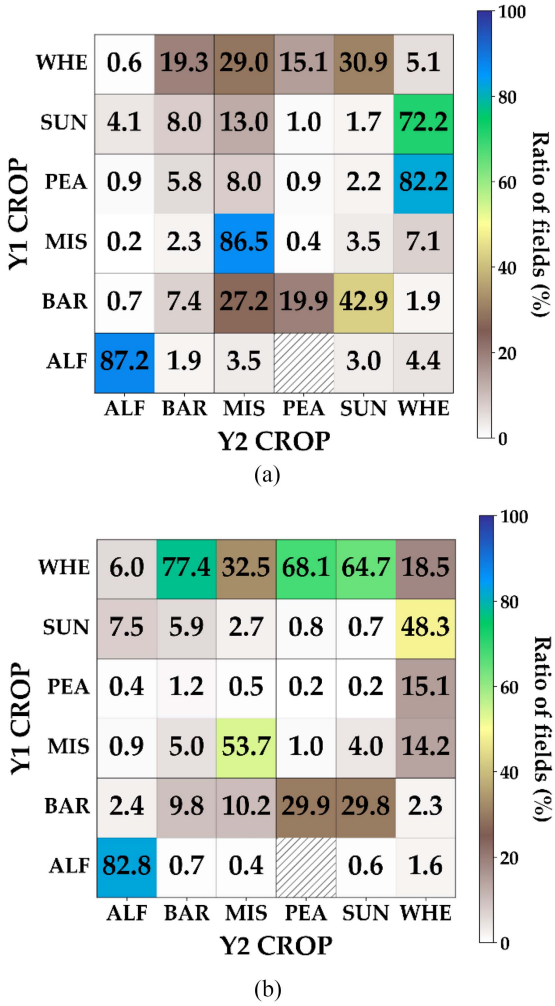

Fig. 13. Matrices showing (a) percentage of Y2 crop as a function of the total of every Y1 crop using data from all classified fields and all the years in our study, (b) percentage of each Y1 crop as a function of the total of every Y2 crop using data from all the years in our study. ALF: alfalfa, WHE: wheat, MAI: maize, BAR: barley, PEA: peas, and SUN: sunflower. (a) reads horizontally and (b) reads vertically.

before cover crops with 40.5% of the total classified fields while maize was the most recurrent crop after cover crops with 34.1%.

Next, and in order to better understand the crop patterns for the classified fields with cover crops, we determined which two crops are commonly paired together in our study period (before and after cover crops). Fig. 13(a) shows the percentage of every Y2 crop in function of the total of every Y1 crop for fields having cover crops. For example, out of all the fields that have sunflower as the Y1 crop, 4.1% of these fields will have alfalfa in Y2, 72.2% will have wheat, 13.0% maize, 8.0% barley, 1.0% peas, and 1.7% sunflower. In addition, Fig. 13(b) shows the percentage of every Y1 crop as a function of the total of every Y2 crop. For example, out of all the fields that have sunflower as the Y2 crop, 0.6% of these fields had alfalfa in Y1, 64.7% had wheat, 4.0% maize, 29.8% barley, 0.2% peas, and 0.7% sunflower.

In Fig. 13(a), we see that when the Y1 crop is alfalfa (ALF), the Y2 crop was mostly alfalfa as well (87.2%). When wheat (WHE) is the Y1 crop, the Y2 crop was more distributed with

the biggest percentage going to sunflower (SUN) with 30.9% and next maize (MAI) with 29.0%. When maize is the Y1 crop, 86.5% of the time the Y2 crop is maize as well. When barley (BAR) is the Y1 crop, sunflower was the most common Y2 crop with 42.9% followed by maize with 27.2%. When the Y1 crop is peas (PEA), 82.2% of Y2 fields had wheat. Finally, when the Y1 crop is sunflower, wheat is the most common Y2 crop with 72.2%.

On the other hand, Fig. 13(b) shows that when the Y2 crop is alfalfa (ALF), the Y1 crop was mostly alfalfa as well (82.8%). When wheat (WHE) is the crop in Y2, Sunflower (SUN) was the Y1 crop most of the time with 48.3%. When maize is the Y2 crop, 53.7% of the time the Y1 crop is maize as well, and when barley (ORG) is the Y2 crop, wheat was the most common Y1 crop with 77.4%. When the Y2 crop is peas (PEA), 68.1% of Y1 fields had wheat. Finally, when the Y1 crop is sunflower, wheat is the most common Y2 crop with 64.7%.

V. Conclusion

Cover cropping is essential in order to capture nitrates and reduce their infiltration into the groundwater. Previous studies have analyzed the potential of optical remote sensing for the mapping of cover crops but very few have utilized SAR remote sensing. The fact that S1 data are available at high temporal and spatial resolutions lends importance to this study by evaluating the potential of SAR remote sensing data in detecting cover crops, especially since it is unaffected by bad weather conditions that are a major limiting factor for optical remote sensing during the growth period of crop cover.

Our classification method is based on the decision tree using the S1 time series data. The decision tree proposed in this study performed well in detecting cover crop fields with recall values ranging from 83.5% to 95.0%. In addition, a high Precision was achieved with values ranging between 81.5% and 89.2% as well as high Kappa values ranging between 0.72 and 0.89. These results show that we are capable of mapping cover crops with high accuracy using solely remote sensing data from SAR S1, whereas most other classification methods are based either on optical remote sensing data alone or on a combination of optical and SAR remote sensing data. Some limitations in detecting cover crops using S1 data were identified. First, although our decision tree method is designed to accommodate a variety of planting times, strategies, and types of cover crops (by using wide windows), this type of classifier might need to be adapted based on the agricultural context in each region and planting strategies (only for regions that are much different from our own). Second, false negatives (failing to detect a cover crop) were found to be due to the low density of the cover crop, resulting in a low vegetation contribution in the total signal. False positives (detecting cover crops where it does not exist) were due mainly due to the existence of vegetation residues in the case when farmers leave the vegetation of the soil after the harvest (used as mulch) and due to increased surface roughness caused by deep plowing after harvesting the principal crop.

The results of our study present two main findings: the first is that we are capable of remotely monitoring cover crops, without the need for expensive ground campaigns, in order to see if farmers are applying healthy agricultural practices or not which is a step forward toward macromanagement of agricultural areas and an important tool when dealing with large-scale agricultural strategies and goals. Second, the mapping of cover crops can be used alongside other agriculture databases such as the RPG in France in order to better understand the prevalence of cover cropping within a certain area.

Acknowledgment

The authors would like to thank Envilys and the staff of the Agglomeration of La Rochelle community and the Eau 17 Water Syndicate for data collecting and access. The authors would also like to thank the European Space Agency for providing the S1 images and the French Land Data Center (Theia) for providing the S2 images.

References

[1] E. F. Lambin and P. Meyfroidt, "Global land use change, economic globalization, and the looming land scarcity," in *Proc. Nat. Acad. Sci., Nat. Acad Sci.*, 2011, pp. 3465–3472.
[2] D. Tilman and M. Clark, "Food, agriculture & the environment: Can we feed the world and save the Earth?," *Daedalus*, vol. 144, no. 4, pp. 8–23, 2015.
[3] K. Wick, C. Heumesser, and E. Schmid, "Groundwater nitrate contamination: Factors and indicators," *J. Environ. Manage.*, vol. 111, pp. 178–186, 2012.
[4] D. C. Bouchard, M. K. Williams, and R. Y. Surampalli, "Nitrate contamination of groundwater: Sources and potential health effects," *J.-Amer. Water Works Assoc.*, vol. 84, no. 9, pp. 85–90, 1992.
[5] E. Moore et al., "The human costs of nitrate-contaminated drinking water in the San Joaquin Valley," *Environ. Health Perspectives*, vol. 119, pp. 1272–1278, 2011.
[6] J. A. Camargo and Á. Alonso, "Ecological and toxicological effects of inorganic nitrogen pollution in aquatic ecosystems: A global assessment," *Environ. Int.*, vol. 32, no. 6, pp. 831–849, 2006.
[7] M. Lunau, M. Voss, M. Erickson, C. Dziallas, K. Casciotti, and H. Ducklow, "Excess nitrate loads to coastal waters reduces nitrate removal efficiency: Mechanism and implications for coastal eutrophication," *Environ. Microbiol.*, vol. 15, no. 5, pp. 1492–1504, 2013.
[8] H. Kirchmann, A. E. J. Johnston, and L. F. Bergström, "Possibilities for reducing nitrate leaching from agricultural land," *Ambi*, vol. 31, no. 5, pp. 404–408, Aug. 2002, doi: 10.1579/0044-7447-31.5.404.
[9] J. J. Meisinger, J. A. Delgado, and A. K. Alva, "Nitrogen leaching management," *Encyclopedia Soils Environ.*, vol. 2, pp. 1122–1124, 2006.
[10] R. Thapa, S. B. Mirsky, and K. L. Tully, "Cover crops reduce nitrate leaching in agroecosystems: A global meta-analysis," *J. Environ. Qual.*, vol. 47, no. 6, pp. 1400–1411, 2018.
[11] E. J. Kladivko et al., "Cover crops in the upper Midwestern United States: Potential adoption and reduction of nitrate leaching in the Mississippi River basin," *J. Soil Water Conservation*, vol. 69, no. 4, pp. 279–291, 2014.
[12] G. S. Francis, K. M. Bartley, and F. J. Tabley, "The effect of winter cover crop management on nitrate leaching losses and crop growth," *J. Agricultural Sci.*, vol. 131, no. 3, pp. 299–308, 1998.
[13] F. Lemessa and M. Wakjira, "Cover crops as a means of ecological weed management in agroecosystems," *J. Crop Sci. Biotechnol.*, vol. 18, no. 2, pp. 123–135, Jun. 2015, doi: 10.1007/s12892-014-0085-2.
[14] D. C. Reicosky and F. Forcella, "Cover crop and soil quality interactions in agroecosystems," *J. Soil Water Conservation*, vol. 53, no. 3, pp. 224–229, Jul. 1998.
[15] D. Knowler and B. Bradshaw, "Farmers' adoption of conservation agriculture: A review and synthesis of recent research," *Food Policy*, vol. 32, no. 1, pp. 25–48, Feb. 2007, doi: 10.1016/j.foodpol.2006.01.003.

[16] J. Constantin et al., "Effects of catch crops, no till and reduced nitrogen fertilization on nitrogen leaching and balance in three long-term experiments," *Agriculture, Ecosyst. Environ.*, vol. 135, no. 4, pp. 268–278, 2010, doi: https://doi.org/10.1016/j.agee.2009.10.005.

[17] C. De Notaris, J. Rasmussen, P. Sørensen, and J. E. Olesen, "Nitrogen leaching: A crop rotation perspective on the effect of N surplus, field management and use of catch crops," *Agriculture, Ecosyst. Environ.*, vol. 255, pp. 1–11, 2018.

[18] T. Rinnofner, J. K. Friedel, R. De Kruijff, G. Pietsch, and B. Freyer, "Effect of catch crops on N dynamics and following crops in organic farming," *Agronomy Sustain. Develop.*, vol. 28, pp. 551–558, 2008.

[19] S. Carlson and R. Stockwell, "Research priorities for advancing adoption of cover crops in agriculture-intensive regions," *J. Agriculture, Food Syst., Community Develop.*, vol. 3, no. 4, pp. 125–129, Aug. 2013, doi: 10.5304/jafscd.2013.034.017.

[20] J. N. Galloway et al., "Transformation of the nitrogen cycle: Recent trends, questions, and potential solutions," *Science*, vol. 320, no. 5878, pp. 889–892, 2008.

[21] N. Gruber and J. N. Galloway, "An earth-system perspective of the global nitrogen cycle," *Nature*, vol. 451, no. 7176, pp. 293–296, 2008.

[22] S. M. Dabney, "Cover crop impacts on watershed hydrology," *J. Soil Water Conservation*, vol. 53, no. 3, pp. 207–213, 1998.

[23] M. Askegaard, J. E. Olesen, and K. Kristensen, "Nitrate leaching from organic arable crop rotations: Effects of location, manure and catch crop," *Soil Use Manage.*, vol. 21, no. 2, pp. 181–188, 2005.

[24] A. Nouri, S. Lukas, S. Singh, S. Singh, and S. Machado, "When do cover crops reduce nitrate leaching? A global meta-analysis," *Glob. Change Biol.*, vol. 28, no. 15, pp. 4736–4749, 2022.

[25] S. A. Wood and M. Bowman, "Large-scale farmer-led experiment demonstrates positive impact of cover crops on multiple soil health indicators," *Nature Food*, vol. 2, no. 2, pp. 97–103, 2021.

[26] P. W. Unger and M. F. Vigil, "Cover crop effects on soil water relationships," *J. Soil Water Conservation*, vol. 53, no. 3, pp. 200–207, Jul. 1998.

[27] P. J. Pinter Jr et al., "Remote sensing for crop management," 2003. [Online]. Available: https://digitalcommons.unl.edu/usdaarsfacpub/1372

[28] M. Shoshany, "Satellite remote sensing of natural Mediterranean vegetation: A review within an ecological context," *Prog. Phys. Geogr.*, vol. 24, no. 2, pp. 153–178, 2000.

[29] D. Lu, "The potential and challenge of remote sensing-based biomass estimation," *Int. J. Remote Sens.*, vol. 27, no. 7, pp. 1297–1328, 2006.

[30] L. Wang and J. J. Qu, "NMDI: A normalized multi-band drought index for monitoring soil and vegetation moisture with satellite remote sensing," *Geophysical Res. Lett.*, vol. 34, no. 20, 2007, Art. no. 251205.

[31] N. Pettorelli, J. O. Vik, A. Mysterud, J. -M. Gaillard, C. J. Tucker, and N. C. Stenseth, "Using the satellite-derived NDVI to assess ecological responses to environmental change," *Trends Ecol. Evol.*, vol. 20, no. 9, pp. 503–510, 2005.

[32] R. S. Lunetta, J. F. Knight, J. Ediriwickrema, J. G. Lyon, and L. D. Worthy, "Land-cover change detection using multi-temporal MODIS NDVI data," *Remote Sens. Environ.*, vol. 105, no. 2, pp. 142–154, 2006.

[33] C. Senf, P. J. Leitão, D. Pflugmacher, S. van der Linden, and P. Hostert, "Mapping land cover in complex Mediterranean landscapes using Landsat: Improved classification accuracies from integrating multi-seasonal and synthetic imagery," *Remote Sens. Environ.*, vol. 156, pp. 527–536, 2015.

[34] N. Kussul, M. Lavreniuk, S. Skakun, and A. Shelestov, "Deep learning classification of land cover and crop types using remote sensing data," *IEEE Geosci. Remote Sens. Lett.*, vol. 14, no. 5, pp. 778–782, May 2017.

[35] B. D. Wardlow, S. L. Egbert, and J. H. Kastens, "Analysis of time-series MODIS 250 m vegetation index data for crop classification in the US Central Great Plains," *Remote Sens. Environ.*, vol. 108, no. 3, pp. 290–310, 2007.

[36] A. B. Baloloy et al., "Estimation of mangrove forest aboveground biomass using multispectral bands, vegetation indices and biophysical variables derived from optical satellite imageries: Rapideye, Planetscope and Sentinel-2," *ISPRS Ann. Photogramm., Remote Sens. Spatial Inf. Sci.*, vol. 4, pp. 29–36, 2018.

[37] S. Ghosh, D. R. Mishra, and A. A. Gitelson, "Long-term monitoring of biophysical characteristics of tidal wetlands in the northern gulf of Mexico—A methodological approach using MODIS," *Remote Sens. Environ.*, vol. 173, pp. 39–58, 2016.

[38] K. Prabhakara, W. D. Hively, and G. W. McCarty, "Evaluating the relationship between biomass, percent groundcover and remote sensing indices across six winter cover crop fields in Maryland, United States," *Int. J. Appl. Earth Observ. Geoinf.*, vol. 39, pp. 88–102, 2015.

[39] P. Thanh Noi and M. Kappas, "Comparison of random forest, k-nearest neighbor, and support vector machine classifiers for land cover classification using Sentinel-2 imagery," *Sensors*, vol. 18, no. 1, 2017, Art. no. 18.

[40] H. Zheng et al., "Performance evaluation of downscaling Sentinel-2 imagery for land use and land cover classification by spectral-spatial features," *Remote Sens.*, vol. 9, no. 12, 2017, Art. no. 1274.

[41] C. Schulz, A. -K. Holtgrave, and B. Kleinschmit, "Large-scale winter catch crop monitoring with Sentinel-2 time series and machine learning–An alternative to on-site controls?," *Comput. Electron. Agriculture*, vol. 186, 2021, Art. no. 106173, doi: 10.1016/j.compag.2021.106173.

[42] J. Betbeder, S. Rapinel, S. Corgne, E. Pottier, and L. Hubert-Moy, "TerraSAR-X dual-pol time-series for mapping of wetland vegetation," *ISPRS J. Photogramm. Remote Sens.*, vol. 107, pp. 90–98, 2015, doi: 10.1016/j.isprsjprs.2015.05.001.

[43] X. Jiao, H. McNairn, J. Shang, and J. Liu, "The sensitivity of multi-frequency (X, C and L-band) radar backscatter signatures to bio-physical variables (LAI) over corn and soybean fields," *Int. Arch. Photogramm., Remote Sens. Spatial Inf. Sci., ISPRS Arch.*, vol. 38, pp. 317–321, Jan.–2010.

[44] J. Betbeder, S. Rapinel, T. Corpetti, E. Pottier, S. Corgne, and L. Hubert-Moy, "Multitemporal classification of TerraSAR-X data for wetland vegetation mapping," *J. Appl. Remote Sens.*, vol. 8, no. 1, Apr. 2014, Art. no. 083648, doi: 10.1117/1.JRS.8.083648.

[45] M. Vreugdenhil et al., "Sensitivity of Sentinel-1 backscatter to vegetation dynamics: An Austrian case study," *Remote Sens.*, vol. 10, no. 9, Sep. 2018, Art. no. 9, doi: 10.3390/rs10091396.

[46] K. Van Tricht, A. Gobin, S. Gilliams, and I. Piccard, "Synergistic use of radar Sentinel-1 and optical Sentinel-2 imagery for crop mapping: A case study for Belgium," *Remote Sens.*, vol. 10, no. 10, Oct. 2018, Art. no. 10, doi: 10.3390/rs10101642.

[47] M. J. Steinhausen, P. D. Wagner, B. Narasimhan, and B. Waske, "Combining Sentinel-1 and Sentinel-2 data for improved land use and land cover mapping of monsoon regions," *Int. J. Appl. Earth Observ. Geoinf.*, vol. 73, pp. 595–604, 2018, doi: https://doi.org/10.1016/j.jag.2018.08.011.

[48] D. Ho Tong Minh et al., "Deep recurrent neural networks for winter vegetation quality mapping via multitemporal SAR Sentinel-1," *IEEE Geosci. Remote Sens. Lett.*, vol. 15, no. 3, pp. 464–468, Mar. 2018, doi: 10.1109/LGRS.2018.2794581.

[49] H. Bazzi, N. Baghdadi, I. Fayad, M. Zribi, H. Belhouchette, and V. Demarez, "Near real-time irrigation detection at plot scale using Sentinel-1 data," *Remote Sens.*, vol. 12, no. 9, 2020, Art. no. 1456.

[50] H. Bazzi et al., "Mapping irrigated areas using Sentinel-1 time series in Catalonia, Spain," *Remote Sens.*, vol. 11, no. 15, Jan. 2019, Art. no. 15, doi: 10.3390/rs11151836.

[51] H. Bazzi et al., "Detecting irrigation events over semi-arid and temperate climatic areas using sentinel-1 data: Case of several summer crops," *Agronomy*, vol. 12, no. 11, Nov. 2022, Art. no. 11, doi: 10.3390/agronomy12112725.

[52] H. Bazzi, N. Baghdadi, I. Fayad, F. Charron, M. Zribi, and H. Belhouchette, "Irrigation events detection over intensively irrigated grassland plots using Sentinel-1 data," *Remote Sens.*, vol. 12, no. 24, Jan. 2020, Art. no. 24, doi: 10.3390/rs12244058.

[53] N. Baghdadi, M. Bernier, R. Gauthier, and I. Neeson, "Evaluation of C-band SAR data for wetlands mapping," *Int. J. Remote Sens.*, vol. 22, no. 1, pp. 71–88, 2001.

[54] R. d'Andrimont, M. Taymans, G. Lemoine, A. Ceglar, M. Yordanov, and M. van der Velde, "Detecting flowering phenology in oil seed rape parcels with Sentinel-1 and -2 time series," *Remote Sens. Environ.*, vol. 239, Mar. 2020, Art. no. 111660, doi: 10.1016/j.rse.2020.111660.

[55] J. Han et al., "The RapeseedMap10 database: Annual maps of rapeseed at a spatial resolution of 10 m based on multi-source data," *Earth Syst. Sci. Data*, vol. 13, no. 6, pp. 2857–2874, 2021.

[56] A. Veloso et al., "Understanding the temporal behavior of crops using Sentinel-1 and Sentinel-2-like data for agricultural applications," *Remote Sens. Environ.*, vol. 199, pp. 415–426, 2017, doi: https://doi.org/10.1016/j.rse.2017.07.015.

[57] D. L. Olson and D. Delen, *Advanced Data Mining Techniques*. New York, NY, USA: Springer, 2008.

[58] N. Baghdadi, C. King, A. Bourguignon, and A. Remond, "Potential of ERS and RADARSAT data for surface roughness monitoring over bare agricultural fields: Application to catchments in Northern France," *Int. J. Remote Sens.*, vol. 23, no. 17, pp. 3427–3442, 2002.

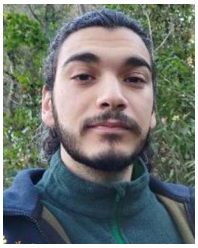

Sami Najem received the master's degree in management and conservation of natural resources from Lebanese University, Fanar, Lebanon, in 2019.

His master's thesis was centered around drought monitoring in the MENA region using radar microwave remote sensing data. He is currently a Research Engineer with INRAE UMR-TETIS, Montpellier, France. His research interests include Earth observation using radar and optical remote sensing in the fields of agriculture and water management.

Nicolas Baghdadi received the Ph.D. degree in estimation of coastal currents using remote sensing from the University of Toulon, La Valette-du-Var, France, in 1994.

From 1995 to 1997, he was a Postdoctoral Researcher with INRS Ete – Water Earth Environment Research Centre, Quebec University, Canada. From 1998 to 2008, he was with French Geological Survey, Orléans, France. Since 2008, he has been a Senior Scientist with the National Research Institute for Agriculture, Food and the Environment, Montpellier, France. His research activities include the areas of microwave remote sensing, image processing, and satellite and airborne remote sensing data analysis. His main field of interest is the analysis of remote sensing data (SAR, Lidar, optical) and the retrieval of environmental parameters (e.g., soil moisture content, surface roughness, irrigation, canopy height, biomass, etc.). He was the Scientific Director of the French Land Data Centre (Theia) from 2014 to 2021. He has authored or coauthored more than 200 articles in refereed journals. He is an Editor of 20 books about remote sensing theory and applications. He has acquired strong experience in the design and management of national and international research projects.

Hassan Bazzi received the Ph.D. degree in remote sensing from AgroParisTech University, Montpellier, France, within the UMR TETIS in 2021.

He is the Head of the Innovation Lab, Atos-Paris. He is managing an integrated team between Atos and the Laboratory of Climate and Environmental Science, University of Paris-Saclay, focusing on research for carbon and agricultural monitoring. His research area focuses on land surface monitoring using Earth observation data, including optical and microwave remote sensing. Since 2017, he has been working on various applications of remote sensing, focusing on image processing, remote sensing data analysis, and the development of machine learning-based methods applied to hydrology, agronomy, and most recently greenhouse gas modeling.

Nathalie Lalande received the Ph.D. degree in environmental science from AgroParistech and the Université of Montpellier, Montpellier, France, in 2013.

Since 2014, she has been working as an R&D Project Manager for the preservation of the quality of drinking water. Her research interests deal with the interactions between land use and the transfer of pollutants to water resources (surface water and groundwater). In strong interaction with water resource managers, she leads numerous collaborations with institutional research organizations on the establishment of remote sensing chains and the modeling of pollutant transfers to water resources. These collaborations resulted in several publications with researchers.

Laurent Bouchet received the graduation degree in agricultural engineering from the Agricultural Engineering School, SupAgro, Montpellier, France, in 2003.

He cofounded the company Envilys in 2005. For more than 20 years, he has supported stakeholders in to fight against the pollution of water resources. He puts his expertise and professional knowledge at the service of national scientific working groups. Since the creation of the company, he has maintained close relationships with the scientific community. The company and its professional expertise make it possible to test and support the use of tools developed by environmental researchers.